IOPscience iopscience.iop.org

Home Search Collections Journals About Contact us My IOPscience

Surface energy enhanced crystallization kinetics in ultrathin foils of amorphous alloys

This article has been downloaded from IOPscience. Please scroll down to see the full text article.

1998 J. Phys.: Condens. Matter 10 8671

(http://iopscience.iop.org/0953-8984/10/39/006)

View the table of contents for this issue, or go to the journal homepage for more

Download details:
IP Address: 171.66.16.210
The article was downloaded on 14/05/2010 at 17:24

Please note that terms and conditions apply.

J. Phys.: Condens. Matter **10** (1998) 8671–8678. Printed in the UK PII: S0953-8984(98)90721-4

Surface energy enhanced crystallization kinetics in ultrathin foils of amorphous alloys

G Schumacher† and R P Wahi‡

† Technical University Berlin, Institute of Metallic Materials, Hardenbergstrasse 36, D-10623 Berlin, Germany

‡ Hahn–Meitner Institute Berlin, Glienicker Strasse 100, D-14109 Berlin, Germany

Received 15 January 1998, in final form 3 June 1998

Abstract. A thermodynamic description of crystallization in amorphous thin foils is presented. The specimen geometry is described by a wedge and the total driving force for phase transformation is expressed in terms of volume, surface and interfacial free energies. At low specimen thickness, the driving force is strongly enhanced by the surface free energy and approaches a constant value at large specimen thickness which is determined by the volume free energy. Energy minimizing crystal orientation results in equiaxed crystals at low specimen thickness. The classical theory of phase transformation is used to calculate the crystallization rate. The results of the present work show that the crystallization rate increases strongly at low specimen thickness which is in qualitative agreement with experimental results.

1. Introduction

The application of metastable amorphous thin films requires knowledge of their thermal stability because many physical properties deteriorate during the transformation to the crystalline state. Though considerable knowledge exists on the stability of amorphous metals, little is known about the influence of the specimen surface and of the substrate/layer interface on crystallization of thin amorphous films. *In situ* studies of electrochemically thinned specimens in a transmission electron microscope (TEM) are useful to provide information about the influence of the free surface on the thermal stability of thin amorphous films. Köster [1] detected by means of TEM that $Fe_{78}Mo_2B_{20}$ and $Fe_{80}B_{20}$ glasses crystallize differently in thin and thick specimens. This was ascribed to a shift of the boundaries in the phase diagram by the surface free energy which changes the total free energy of the system [1].

In amorphous $Ni_{80}P_{20}$ and $Ni_{69}Cr_{14}P_{17}$ alloys, the crystallization process was found to depend on the specimen thickness in the following way. In thick parts of specimens (thickness h larger than 50 nm) thinned electrochemically for TEM, crystallization proceeds in two steps via: (i) primary crystallization of phosphorus-poor fcc Ni [2] and Ni–Cr [3] precipitates, respectively, and (ii) subsequent polymorphous crystallization of the phosphorus-enriched amorphous matrix into the stable tetragonal Ni_3P [2] and $(Ni, Cr)_3P$ [3] phases, respectively. In very thin parts of the specimens (h smaller than 50 nm) crystallization starts earlier and proceeds in a completely different way via the formation of metastable hexagonal phases of composition Ni_3P [2] and $(Ni, Cr)_3P$ [3], respectively. The c-axis of these phases is always perpendicular to the specimen surface. Crystallization starts at the thinnest region of the specimen, i.e. directly at the perforation edge of the

0953-8984/98/398671+08$19.50 © 1998 IOP Publishing Ltd

TEM specimen, and the crystallization front is parallel to the perforation edge [2, 3]. At short annealing times, i.e. close to the perforation edge, the crystallization rate of the hexagonal $(Ni, Cr)_3P$ phase was found to be about one order of magnitude higher than at larger annealing times at which the crystallization rate is constant within the experimental uncertainty [3]. These results hint at an approximately constant driving force for phase transformation in thicker parts of the specimens and an increase in the driving force at smaller specimen thickness. The crystallization rate in $Ni_{80}P_{20}$ was measured only at short annealing times, i.e. in very thin ranges. In this range, a linear time dependence of crystal growth was observed [2]. At higher temperatures the metastable hexagonal Ni_3P and $(Ni, Cr)_3P$ phases transform into the corresponding stable tetragonal phases [2, 3].

Influences of the specimen thickness on the thermal stability were also found in ultrathin foils of amorphous $Pd_{81}Si_{19}$ [4]. It was found that crystal nucleation starts at the perforation edge, i.e. at the thinnest parts of the specimen. After impingement of neighbouring crystals, a crystallization front formed which was aligned parallel to the perforation edge and which proceeded in the direction perpendicular to the perforation edge [4]. While the composition of the crystalline phase was determined to be close to the composition of the amorphous phase, the crystal structure was in agreement with the crystal structure of the hexagonal Pd_2Si phase.

The results obtained from studies of crystallization in ultrathin foils of amorphous $Pd_{81}Si_{19}$, $Ni_{80}P_{20}$ and $Ni_{69}Cr_{14}P_{17}$ point to appreciable shifts in the phase boundaries and to a reduction in the thermal stability at small specimen thickness.

This paper presents a thermodynamic description of crystal growth in amorphous alloys at low specimen thickness.

2. The model

The shape of the specimen is described by a wedge. The wedge angle α is included by the upper and lower free surface which intersect at the edge (figure 1). The length of a crystal which is located at the edge of the wedge and impinges with neighbouring crystals at the upper and lower end is denoted by L and the widths at the surface and at $\alpha/2$ are denoted by b and x, respectively. At small angles α, the widths x and b are approximately the same. For a stress equilibrated surface, the specific surface free energies Γ_a and Γ_{cr} of the amorphous and of the crystalline state, respectively, are related to the specific free energy of the amorphous–crystalline interface, Γ_{a-cr}, by

$$\Gamma_a = \Gamma_{cr} + \Gamma_{a-cr}\cos(90^\circ - (\Phi + \alpha/2)). \tag{1}$$

The angle Φ determines the radius of curvature R of the amorphous–crystalline interface by $\sin\Phi = h/(2R)$ where h denotes the local specimen thickness at x.

The surface free energies of neighbouring crystals are assumed to be identical, resulting in planar crystalline–crystalline interfaces. Each of the two surface areas is given by $A_1 = bL$. For small angles α and Φ, the interface areas A_2 and A_3 parallel and perpendicular to the edge of the wedge can approximately be described by Lh and $bh/2$, respectively. The change in free energy with changing crystal size can then be expressed by

$$\mathrm{d}\Delta G = \mathrm{d}V\,\Delta G^v + 2\,\mathrm{d}A_1(\Gamma_a - \Gamma_{cr}) - \mathrm{d}A_2\Gamma_{a-cr} - \mathrm{d}A_3\Gamma_{cr-cr} \tag{2}$$

where $\Delta G = G_a - G_{cr}$ denotes the difference in the total free energy between the amorphous (G_a) and the crystalline (G_{cr}) state, $\Delta G^v = G_a^v - G_{cr}^v$ is the difference in the specific volume free energy between the amorphous and the crystalline state and Γ_{a-cr} and Γ_{cr-cr} denote the specific interfacial free energies of the amorphous–crystalline interface and of

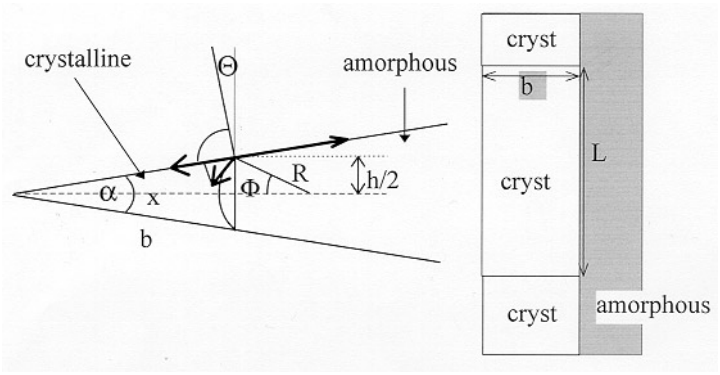

Figure 1. Schematic representation of a wedge shaped specimen: (a) side view; (b) top view. The arrows indicate the directions of the surface and interfacial tensions.

the crystalline–crystalline interface, respectively. Only one of the crystalline–crystalline interfaces is assigned to the crystal of consideration.

The transformation from the amorphous to the crystalline state is generally accompanied by an increase in mass density of the order of 2%, resulting in elastic strains at both sides of the amorphous–crystalline interface. The resulting strain energies are expected to be proportional to the interface area while the ranges of the strains perpendicular to the interface in the crystalline and amorphous state may be described by characteristic lengths λ_{cr} and λ_a, respectively. For $\lambda_{cr} > x$, the total strain energy of the amorphous–crystalline interface may then be given by $\lambda_{cr} hL\gamma_{cr} + \lambda_a hL\gamma_a$ where γ_{cr} and γ_a are the elastic strain energy densities of the crystalline and the amorphous state, respectively. For simplicity, the strain energy is neglected in our approach.

A change db in crystal width causes a change $\mathrm{d}h = \mathrm{d}b/k$ in the thickness and a change $\mathrm{d}V = Lkh\,\mathrm{d}h$ in the crystal volume where $k = b/h = 0.5/\sin(\alpha/2)$. Each of the two free surfaces with area A_1 is changed by $\mathrm{d}A_1 = Lk\,\mathrm{d}h$, while the interface areas A_2 and A_3 parallel and perpendicular to the edge are changed by $\mathrm{d}A_2 = L\,\mathrm{d}h$ and $\mathrm{d}A_3 = kh\,\mathrm{d}h$, respectively. The driving force for crystallization is then given by

$$-\partial(\Delta G)/\partial V = -\Delta G^v - 2(\Gamma_a - \Gamma_{cr})/h + \Gamma_{a-cr}/(kh) + \Gamma_{cr-cr}/L. \qquad (3)$$

For simplicity, interfaces perpendicular to the edge of the wedge which separate neighbouring crystals are assumed to be planar. This results in crystals of constant length. While Γ_{cr} and Γ_{cr-cr} depend on the crystal orientation, described by three angles Θ, β and ε relative to a given co-ordinate system, the value of Γ_{a-cr} is assumed to be independent of crystal orientation. For simplicity, the present description of crystal orientation is restricted to one orientation degree of freedom in a way that $\Gamma_{cr}(\Theta, \beta, \varepsilon) = \Gamma_{cr}(\Theta)$.

At sufficiently high temperatures, out-of-surface-plane stresses caused by the amorphous–crystalline interfaces might be equilibrated by the formation of grooves at triple junctions in analogy to thermal grooving in pure crystalline materials [5]. For simplicity, the process of grooving is neglected in the present considerations.

In the following we assume that $L \gg h$. The last term on the right-hand side of (3) can then be neglected, because Γ_{a-cr} and Γ_{cr-cr} are of the same order of magnitude. The driving force is then given by

$$-\partial(\Delta G)/\partial V = -\Delta G^v - 2(\Gamma_a - \Gamma_{cr})/h + \Gamma_{a-cr}/(kh). \qquad (4)$$

According to (4) the contribution of the surface to the total driving force decreases with increasing thickness, while the contributions of the interfacial areas to the driving force increase.

Using the approach of (1) for small angles α,

$$\Gamma_a = \Gamma_{cr} + \Gamma_{a-cr} h/(2R) \tag{5}$$

the driving force can be expressed by

$$-\partial(\Delta G)/\partial V = -\Delta G^v - 2(\Gamma_a - \Gamma_{cr})/h \cdot (1 - R/kh) \tag{6}$$

or, in terms of Γ_{a-cr}, by

$$-\partial(\Delta G)/\partial V = -\Delta G^v - \Gamma_{a-cr}/R \cdot (1 - R/kh). \tag{7}$$

(7) shows that the driving force is enhanced by decreasing R. According to (6) and (7), the total driving force is enhanced by the surface and interfacial free energies if $1 - R/(kh)$ is positive, i.e. if $R < kh$. It is diminished if $R > kh$, and it is not affected by the surface and interface if $R = kh$. The last case is realized when the contributions of the surface and interface compensate each other. The criteria deduced from (6) and (7) depend on the local specimen thickness. Using the relation $\sin(\Theta) = h/(2R)$, a specimen thickness independent criterion $\sin(\Theta) > 1/(2k)$ for the enhancement of the total driving force can be deduced. Taking typical values $k = 20$–50 for electrochemically polished specimens [3, 6], Θ_{crit} is determined to be of the order one degree.

Figure 2 shows the term $R/(kh)$ as a function of the angle Θ using a value $k = 50$. For $R/(kh) \ll 1$, i.e. for large angles Θ and for small angles α, the term $R/(kh)$ approaches zero and can therefore be neglected in (6) and (7). (6) and (7) are then given by

$$-\partial(\Delta G)/\partial V = -\Delta G^v - 2(\Gamma_a - \Gamma_{cr})/h \tag{8}$$

and

$$-\partial(\Delta G)/\partial V = -\Delta G^v - \Gamma_{a-cr}/R \tag{9}$$

respectively.

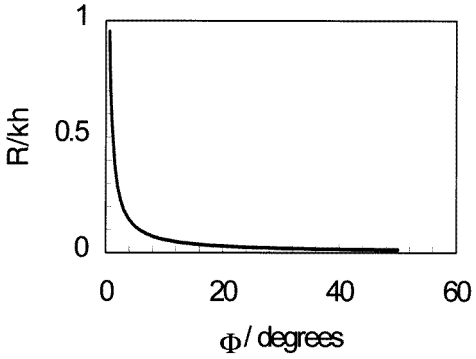

Figure 2. Ratio $R/(kh)$ as a function of the angle Φ.

The surface free energy of a crystal depends sensitively on the crystal orientation [7]. For a wedge shaped crystal, the orientation dependent surface free energy cannot be a minimum with respect to both of the surfaces (see figure 1). Minimization of total free energy requires that the crystal will attain an orientation which minimizes the surface free energy with respect to one of the two surfaces while deviation from the other surface vectors

is given by the angle $\Theta = \alpha$ resulting in an effective surface free energy $\Gamma_{cr}^{eff}(\alpha)$ of the crystal which depends on the wedge angle α (see figure 3). For simplicity, we assume in the following considerations that the crystal takes an orientation which deviates from the energy minimizing orientation of both surfaces by $\Theta = \alpha/2$ resulting in a crystal orientation which is symmetric with respect to both of the surfaces.

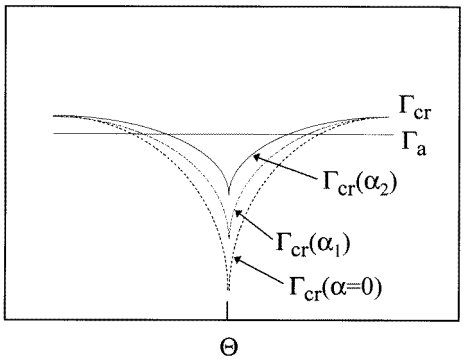

Figure 3. Schematic representation of the surface free energy of an amorphous alloy and its crystalline counterpart in a wedge shaped specimen as a function of Θ (see text) for three wedge angles $\alpha = 0 < \alpha_1 < \alpha_2$.

According to the classical theory of phase transformations [8], the crystal growth rate u during polymorphous crystallization is given by

$$u = a_0 \nu_0 \exp(-Q/RT)[1 - \exp(-\partial(\Delta G)/\partial V/RT)] \tag{10}$$

where a_0 is the width of the interface, ν_0 is a jump frequency of the order of the Debye frequency, T is the temperature, R is the universal gas constant and Q is the activation energy for crystallization.

3. Results and discussion

Figure 4 shows contributions of the volume (— · —), surface (– – –), and of the amorphous–crystalline interface (· · · · · ·) to the driving force according to (4) as a function of the specimen thickness at the crystal width b as well as the sum of these three contributions (solid line) using $\Delta G^v = 1.4 \times 10^8$ J m^{-3} ($\approx$1.5 kJ mol^{-1}), $\Gamma_{a-cr} = 0.3$ J m^{-2} [9, 10] and $\Gamma_a - \Gamma_{cr} = 0.1$ J m^{-2}. The crystal length is assumed to be so large that the driving force of the interfaces perpendicular to the perforation edge can be neglected in (2) and (3). Figure 4 shows that the driving force of the interface parallel to the perforation edge can also be neglected for small wedge angles α. The driving force from the two free surfaces increases strongly at low specimen thickness and approaches zero at large specimen thickness. The total driving force is dominated by the surface free energy at low specimen thickness and approaches $-\Delta G^v$ at large specimen thickness.

Figure 5 shows the crystal growth rate according to (10) in the direction perpendicular to the perforation edge using the driving force given by (8) and using typical parameter values $a_0 = 0.3$ nm, $\nu_0 = 10^{12}$ s^{-1}, $Q = 2.2 \times 10^{10}$ J m^{-3} ($\approx$160 kJ mol^{-1}), $\Delta G^v = 1.4 \times 10^8$ J m^{-3} ($\approx$1 kJ mol^{-1}) and $\Gamma_{a-cr} = 0.3$ J m^{-2} [9, 10]. For k and Φ, the values 50 [6] and $\pi/2$ have been used, respectively. For this value of Φ, the term $R/(kh)$ can be neglected and the driving force is given by (8).

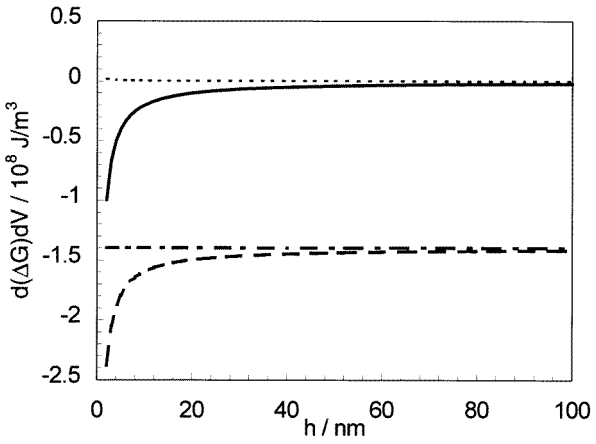

Figure 4. Contributions of the volume (— · —), surface (– – –), and of the amorphous–crystalline interface (· · · · · ·) to the driving force according to (4) as a function of the specimen thickness at the crystal width b as well as the sum of these three contributions (solid line) using $\Delta G^v = 1.4 \times 10^8$ J m^{-3} ($\approx$1.5 kJ mol^{-1}), $\Gamma_{a-cr} = 0.3$ J m^{-2} [9, 10] and $\Gamma_a - \Gamma_{cr} = 0.1$ J m^{-2}.

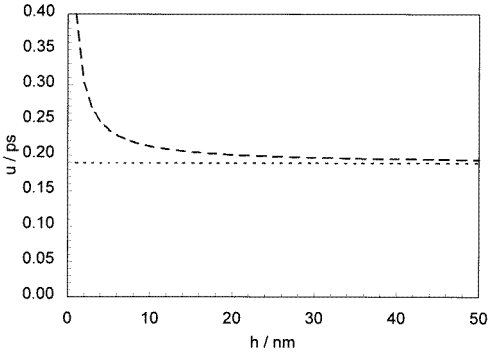

Figure 5. Crystallization rates u for polymorphous crystallization as a function of the specimen thickness for a wedge shaped crystal according to (10) using $a_0 = 0.3$ nm, $\nu_0 = 10^{12}$ s^{-1} and $Q = 160$ kJ mol^{-1} ($\approx 2.2 \times 10^{10}$ J m^{-3} for Ni). The driving force according to (8) was used to determine the crystallization rate. The dashed line represents the crystallization rate for the constant driving force ΔG^v.

The crystallization rate increases at very small specimen thickness due to the surface free energy of the crystal. At large specimen thickness, the crystallization rate approaches a constant value which is determined by ΔG^v.

The results of the present work are in qualitative agreement with the steep increase in crystal growth rate at small specimen thickness observed experimentally in the $Ni_{69}Cr_{14}P_{17}$ alloy [3]. In the thickness range 20 nm to 50 nm the calculated crystal growth rates are approximately constant as it was observed experimentally in the $Ni_{69}Cr_{14}P_{17}$ alloy [3].

The constant crystal growth rate observed experimentally in $Ni_{80}P_{20}$ [2] close to the perforation edge is not confirmed by the results of the present work. The reasons for this discrepancy are not yet clear.

According to (8), the driving force and hence the crystallization kinetics is strongly enhanced at small specimen thickness if the change in surface free energy $\Gamma_a - \Gamma_{cr}$ is large. This obviously is realized for certain crystal orientations as is shown by the formation of equiaxed crystals of the metastable hexagonal phases Ni_3P [2] and $(Ni, Cr)_3P$ [3] where the *c*-axis is oriented perpendicular to the specimen surface. At this orientation, the surface of the hexagonal crystal is built up by densely packed [0001] planes which minimize $\Gamma_{cr}(\Theta)$. Though the specific volume free energy of the metastable phase ΔG_m^v is smaller than the corresponding value ΔG_s^v of the stable phase, the metastable phase can energetically be more favourable at low specimen thickness due to the large value of $2\Delta\Gamma_m/h$. Here, $\Delta\Gamma_m$ denotes the difference $\Gamma_a - \Gamma_{cr}$ for the metastable phase. At larger specimen thickness, the value of $2\Delta\Gamma_m/h$ decreases until at a critical specimen thickness, h_{crit}, the total driving forces of the metastable and stable phase are equal:

$$\delta(\Delta G_m)/\delta V = \delta(\Delta G_s)/\delta V \tag{11}$$

where $\delta(\Delta G_s)/\delta V = \Delta G_m^v + 2\Delta\Gamma_m/h_{crit}$. The indices *m* and *s* denote the metastable and the stable state, respectively.

In the present analysis, typical physical parameters Q, ΔG^v, $\Gamma_a - \Gamma_{cr}$ and Γ_{a-cr} were used. The results of the present work depend, although not critically, on the magnitude of these parameters. No qualitative changes in the results are expected by reasonable alterations of the parameters. It is however obvious that the influence of the surface free energy on crystallization kinetics is enhanced by the low value of ΔG^v and by large values of $\Gamma_a - \Gamma_{cr}$, while (for large *k*) Γ_{a-cr} hardly affects crystallization kinetics.

While the description of crystallization kinetics by means of the thermodynamic framework presented in the present work is straightforward, the description of crystal nucleation provides more difficulties because crystal growth is not only in the direction perpendicular to the edge of the wedge but can also proceed parallel to the edge of the wedge. Crystal nucleation hence depends not only on one co-ordinate but requires a more complex description incorporating the description of the driving force as a function of crystal width and crystal length. In order to describe crystal growth in the direction parallel to the edge of the wedge prior to impingement with other crystals, the crystalline–crystalline interfaces have to be substituted by crystalline–amorphous interfaces.

One might ask whether a wedge shaped crystal geometry is appropriate at all to describe the shape of a crystal in the early stages. On the other hand, homogeneous nucleation in the bulk where only a few atoms agglomerate to form a crystal is approximately described by spherical crystals.

4. Summary and conclusions

A thermodynamic description of polymorphous crystallization in ultrathin foils is presented. The specimen geometry is described by a wedge. The driving force for phase transformation is expressed in terms of the volume, surface and interfacial free energy. The driving force is enhanced by energy minimizing crystal orientation leading to equiaxed crystals in ultrathin ranges of the specimen. While the driving force is dominated by the surface free energy at low specimen thickness, it approximates the value of the volume free energy at large specimen thickness. The experimentally observed effect, that a metastable phase forms at the edge of the wedge and grows until a critical thickness is achieved at which it impinges with crystals of a stable phase is ascribed to the vanishing influence of the surface free energy at larger specimen thickness. Using typical values of the thermodynamic parameters, calculations according to the classical theory of phase transformations yields a crystal growth

rate which increases severely close to the edge of the wedge while it approximates a constant value far away from the edge.

The results of the present work confirm qualitatively the steep increase in the crystal growth rate observed experimentally in very thin ranges of glassy $Ni_{69}Cr_{14}P_{17}$ alloy. The crystal growth rate at larger specimen thickness is not constant as detected experimentally in glassy $Ni_{69}Cr_{14}P_{17}$ alloy but decreases slightly with increasing specimen thickness. Experimental results obtained close to the perforation edge of jet polished $Ni_{80}P_{20}$ specimens where a constant crystallization rate was found [2] are not confirmed by the present work.

The results of the present work are valid for amorphous alloys which crystallize polymorphously, or for alloys where diffusion for at least one alloy component is fast in comparison with the crystallization process. The latter case is obviously realized for the $Ni_{69}Cr_{14}P_{17}$ alloy and for the $Ni_{80}P_{20}$ alloy.

The description of the early stages of crystallization is not as straightforward as the description of crystallization kinetics after impingement of neighbouring crystals because growth of crystal nuclei is considered to proceed differently parallel and perpendicular to the edge of the wedge. A further development of the present description is therefore necessary to incorporate crystal nucleation.

References

[1] Köster U 1979 *Krist. Tech.* **14** 1369
[2] Ikari T, Izahi M, Fukumori T and Futagami K 1991 *J. Mater. Sci.* **26** 538
[3] Schumacher G and Wahi R P 1995 *Scr. Metall. Mater.* **33** 163
[4] Schumacher G and Wahi R P 1998 Phase transformations and systems driven far from equilibrium *Proc. MRS Meeting (Boston, MA, 1997)* vol 481, ed E Ma *et al* (Pittsburgh, PA: Materials Research Society) pp 477–82
[5] Murr L E 1975 *Interfacial Phenomena in Metals and Alloys* (London: Addison-Wesley) p 42
[6] Kelly P M, Jostons A, Blake R G and Napier J G 1975 *Phys. Status Solidi* **31** 771
[7] Wolf D 1992 *Materials Interfaces, Atomic-level Structure and Properties* ed D Wolf and S Yip (London: Chapman and Hall) p 1
[8] Christian J W 1965 *The Theory of Transformations in Metals and Alloys* (Oxford: Pergamon) p 433
[9] Morris D G 1981 *Acta Metall.* **29** 1213
[10] Nishi Y 1984 *Rapidly Quenched Metals V* ed S Steeb and H Warlimont (Amsterdam: North-Holland) p 231